

Electro-Optic Imaging Fourier Transform Spectrometer

Tien-Hsin Chao
Jet Propulsion Laboratory
4800 Oak Grove Drive, Pasadena CA, 91109

Key Words: Hyperspectral Imaging, solid-state Imaging Fourier transform spectrometer, birefringent phase retarders, liquid crystal achromatic phase switch

ABSTRACT

JPL is developing an innovative compact, low mass, Electro-Optic Imaging Fourier Transform Spectrometer (E-O IFTS) for hyperspectral imaging applications. The spectral region of this spectrometer will be 1 – 2.5 μm (1000 – 4000 cm^{-1}) to allow high-resolution, high-speed hyperspectral imaging applications [1-5]. One application will be the remote sensing of the measurement of a large number of different atmospheric gases simultaneously in the same airmass. Due to the use of a combination of birefringent phase retarders and multiple achromatic phase switches to achieve phase delay, this spectrometer is capable of hyperspectral measurements similar to that of the conventional Fourier transform spectrometer but without any moving parts. In this paper, the principle of operations, system architecture and recent experimental progress will be presented.

1. INTRODUCTION

Traditional Fourier transform spectrometers possess two major advantages over grating, prism, and circular variable filter (CVF) spectrometers. One is the time-multiplexing effect. The Michelson interferometer's single detector views all the wavelengths (within the sensor passband) simultaneously throughout the entire measurement. This effectively lets the detector collect data on each wavelength for the entire measurement time, measuring more photons and therefore, results in higher signal-to-noise ratio, at best for situations where the source is stable. The other is the throughput advantages since the FTS does not need spatial filters (e.g. slit) in the optical light path.

However, Traditional FTIR spectrometers, used in space flight missions, obtain their optical delay by physically translating one or more optical components. The so-called translation mechanism usually dominates the risk, cost, power consumption, and performance of such instruments because:

- 1) Over the course of a 5-year period, tens of millions of strokes will be required, making wear or fatigue a serious risk
- 2) The moving optical element cannot be rigidly held, making it sensitive to vibration and requiring that it be "caged" during launch to prevent damage, adding risk (failure of the caging mechanism to reopen).
- 3) Accelerating and decelerating the optical elements can torque the spacecraft, making it difficult to maintain accurate pointing.

A high-resolution FTIR spectrometer without moving parts therefore represents a substantial improvement in reliability, mission duration, and performance. It also promises to be much smaller in size and mass.

2. ELECTRO-OPTIC IMAGING FOURIER TRANSFORM SPECTROMETER

2.1 PRINCIPLE OF OPERATION AND SYSTEM ARCHITECTURE

This paper describes the design of a novel, high-throughput, liquid-crystal-based IFTS for operation in the infrared spectral band. This approach takes advantage of fast switching ferroelectric or dual-frequency nematic LC modulators to quickly vary the time delay in order to implement fast-acquisition of the time-series data.

As shown in Figure 1a, in a traditional FTS, the critical time delay data is acquired by scanning one mirror within a Michelson interferometer. Post-processing of the output time measurements using Fast Fourier transform (FFT) will retrieve the spectral data. In the new E-O IFTS, the bulky, slow scanning mechanism is replaced with a solid-state time delay design using Electro-Optic (E-O) components as shown in Figure 1b. After the input beams passing through a polarizer and a linear retarder made of a birefringent material, the speed difference in refraction indexes between the ordinary and the extraordinary components will generate a time delay in the two throughput beams.

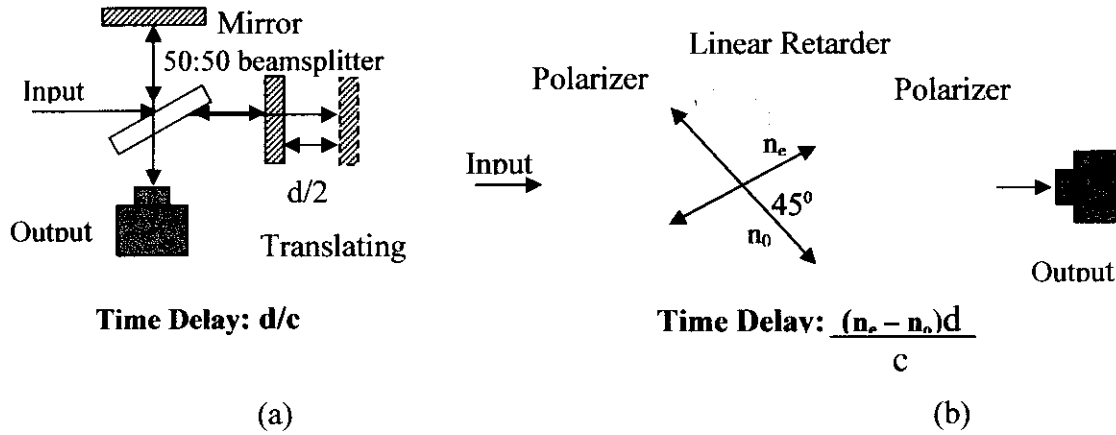


Figure 1. Time delay mechanisms of (a) a Michelson interferometer based FTS; and (b) an E-O solid-state FTS.

As shown in Figure 2, the E-O FT spectrometer would be built upon a sequence of the time-delay unit. It consists an input polarizer, a passive quarter-wave plates (phase shifter), a series of N liquid crystal based electro-optic switches (S_1, S_2, \dots, S_n) interlaced with a series of $(N+1)$ passive birefringent wave retarders ($\Gamma_1, \Gamma_2, \dots, \Gamma_{n+1}$), as described in figure 1a, and an output polarizer. The basic building block of system is the unit consisting of a single achromatic half-wave switch sandwiched between two neighboring passive wave retarders. The principle is that one can select between the sum or difference in total retardation of the wave passing through these two passive wave retarders by rotating the in-between achromatic half-wave switch. With parallel passive retarders oriented at 45 degrees to the input polarization, an achromatic half-wave retarder oriented at 0-degree gives the difference in retardation, while an orientation of 45 degrees gives the sum. By stacking $(n+1)$ passive retarders, with (n) achromatic half-wave switches between them, the 2^n states of the structure represent all combinations of sums and differences of the retardance values. By using a geometric relationship of passive retarder thickness, an arithmetic progression in time delay steps is achieved.

The output of the FTS is a periodic representation of the original bandlimited input spectrum. This periodicity results from the fact that the autocorrelation of the field is sampled to recover the spectrum. Due to the limited number of time-samples, the output spectrum is more accurately a smoothed periodic representation of the input. Knowing this, one can consider the input as a single cycle of the resulting periodic output spectrum. Since the output spectrum is periodic, we can of course express it as a Fourier series

$$S(\omega) = A_0 + \sum_{m=1}^{\infty} A_m \cos\left(\frac{2\pi m \omega}{\Delta\omega}\right) + \sum_{m=1}^{\infty} B_m \sin\left(\frac{2\pi m \omega}{\Delta\omega}\right) \quad (1)$$

Where $\Delta\omega$ is the bandwidth of the spectrum and the Fourier coefficients are given below

$$A_0 = \frac{1}{\Delta\omega} \int_{-\frac{\Delta\omega}{2}}^{\frac{\Delta\omega}{2}} S(\omega) d\omega \quad (2a)$$

$$A_m = \frac{2}{\Delta\omega} \int_{-\frac{\Delta\omega}{2}}^{\frac{\Delta\omega}{2}} S(\omega) \cos\left(\frac{2\pi m\omega}{\Delta\omega}\right) d\omega \quad (2b)$$

$$B_m = \frac{2}{\Delta\omega} \int_{-\frac{\Delta\omega}{2}}^{\frac{\Delta\omega}{2}} S(\omega) \sin\left(\frac{2\pi m\omega}{\Delta\omega}\right) d\omega \quad (2c)$$

The total power on the detector is the integral of the input spectrum modulated by the transmission function of the FTS

$$P = \int_0^{\infty} S(\omega) T(\omega) d\omega = \frac{1}{2} \int_0^{\infty} S(\omega) d\omega + \frac{1}{2} \int_0^{\infty} S(\omega) \cos\left(\frac{2\pi m}{\Delta\omega} \omega + \varphi\right) d\omega \quad (3)$$

Where we have used the transmission function of the FTS that contains active LC switches and multi-order retarders between two polarizers,

$$T = \cos^2\left(\frac{\Gamma}{2} + \frac{\varphi}{2}\right), \quad (4)$$

Where $\Gamma = \frac{\Delta n d}{c} \omega$ is the phase retardation of the multi-order retarder for one stage, determined by its thickness, d , and birefringence, $\Delta n = (n_e - n_o)$. c is the speed of light. φ is a pure phase shift, as provided by an achromatic polarization switch. As described in the above, for multiple stages, the retardation can be stepped in increments of the fundamental τ_0 according to

$$\Gamma = m \tau_0 \omega = \frac{2\pi m}{\Delta\omega} \omega \quad (5)$$

Assume that the achromatic phase shifter φ switches between four states separated by a quarter-wave of retardation (i.e. $\varphi = -\frac{\pi}{2}, 0, \frac{\pi}{2}$ and π), which was done by using the combination of an achromatic half-wave switch (S_{n+1} in Fig. 1) with an achromatic quarter-wave switch ($\lambda/4$ in Fig. 1). For one particular multi-order retardance (m), we generate four power measurements on the detector $P_m^0, P_m^\pi, P_m^{\frac{\pi}{2}}$ and $P_m^{-\frac{\pi}{2}}$. Then, in the window of bandwidth, we have

$$P_m^A = P_m^0 - P_m^\pi = \int_0^{\infty} S(\omega) \cos\left(\frac{2\pi m\omega}{\Delta\omega}\right) d\omega = \int_{\omega_0 - \frac{\Delta\omega}{2}}^{\omega_0 + \frac{\Delta\omega}{2}} S(\omega) \cos\left(\frac{2\pi m\omega}{\Delta\omega}\right) d\omega \quad (6a)$$

$$P_m^B = P_m^{\frac{\pi}{2}} - P_m^{-\frac{\pi}{2}} = \int_0^{\infty} S(\omega) \sin\left(\frac{2\pi m\omega}{\Delta\omega}\right) d\omega = \int_{\omega_0 - \frac{\Delta\omega}{2}}^{\omega_0 + \frac{\Delta\omega}{2}} S(\omega) \sin\left(\frac{2\pi m\omega}{\Delta\omega}\right) d\omega \quad (6b)$$

$$P_0 = P_m^0 + P_m^\pi = P_m^{\frac{\pi}{2}} + P_m^{-\frac{\pi}{2}} = \int_0^{\infty} S(\omega) d\omega = \int_{\omega_0 - \frac{\Delta\omega}{2}}^{\omega_0 + \frac{\Delta\omega}{2}} S(\omega) d\omega \quad (6c)$$

Compared with Eq. (1), the spectrum is constructed by assembling the Fourier series using the sequence of power measurements

$$S(\omega) = \frac{1}{\Delta\omega} \left[P_0 + 2 \sum_{m=1}^{\infty} P_m^A \cos\left(\frac{2\pi m \omega}{\Delta\omega}\right) + 2 \sum_{m=1}^{\infty} P_m^B \sin\left(\frac{2\pi m \omega}{\Delta\omega}\right) \right] \quad (7)$$

This shows that the FTS can, in principle, recover a spectrum. The Fourier coefficients are measured using structures between the polarizers: (1) A digital switch that changes the period of a sinusoidal transmission function in multiples of the input spectral bandwidth, and (2) A four-state achromatic switchable retarder that steps in quarter-wave increments at each order.

The common-path design is physically compact and inherently stable with no moving parts. By replacing precision mechanical movements with low-power binary liquid crystal switches, power supply and packaging requirements are greatly reduced which translates into a large weight reduction. In addition, the common-path approach simplifies the optical design. The in-line optical design reduces size and its mechanical stability and durability. These benefits allow the optical head to be fabricated as a solid block optic with no gaps between elements.

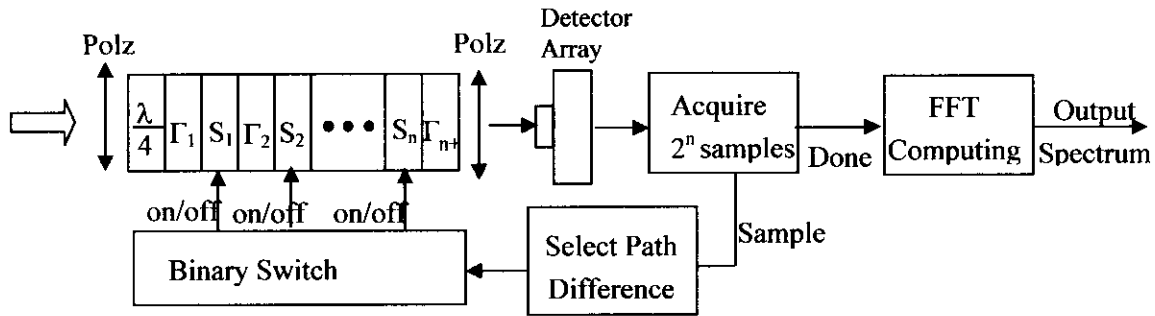


Figure 2. Block diagram of the electro-optic Imaging Fourier transform spectrometer

2.1 SPECTRAL RESOLUTION

Similar to a conventional FTS, the spectral resolution, $\Delta\sigma$, of the proposed EO-FTS is related to the maximum optical path difference, Δx , or equivalently, the maximum time delay, δ_{\max} , between the two interfering waves:

$$\Delta\sigma = \frac{1}{\Delta x_{\max}} = \frac{1}{d \cdot (n_o - n_e)} = \frac{1}{\lambda \cdot 2^N}. \quad \text{If a total of } N \text{ switches (} N \text{ stages) is used, the time delay of each}$$

switch will be approximately $2^0\lambda, 2^1\lambda, \dots, 2^N\lambda$ with maximum time delay $\delta_{\max} \sim 2^N\lambda_{\text{med}}$ where λ_{med} is the central wavelength of the spectral passband). For the proposed spectrum range of $1.0 \sim 2.5\mu\text{m}$, the central wavelength is about $1.8 \mu\text{m}$ (5500 cm^{-1}). Thus the spectral resolution for an 11-stages and a 13-stages EO-FTS will be about 2.68cm^{-1} and 0.67cm^{-1} respectively.

3. DEVELOPMENT OF 8-STAGE IR FTS

We have recently developed a 8stage EOFTS laboratory breadboard and demonstrated preliminary IR spectral data capture and retrieval. Details of this development work including the fabrication and testing of achromatic half-wave FLC switches, optical design, electronics and software development will be presented. The eight-stage IR FTS successfully identified the 1550 nm Diode laser spectrum.

3.1 OPTICAL DESIGN AND SETUP

The setup is sketched in Figure 3a. A Diode laser at 1550 nm wavelength was used as light source and a single silica photodiode (*New Focus*, Model#2011) as the light detector. The signal from the detector was acquired by an A/D board in a computer. Multiple optical delays are generated by eight achromatic half-wave FLC switches (S1, S2,.. S8) put among four passive wave retarders with delays of 1λ , 2λ , 4λ ,... 512λ respectively. The ninth half-wave switch (S4) was used to generate a 0 or π phase retardation. An achromatic $\lambda/4$ switch was used to shift the system to additional $\pm\pi/2$ phase. An interface control program was written to apply voltages (± 5 V) on the FLC switches, and to acquire signals.

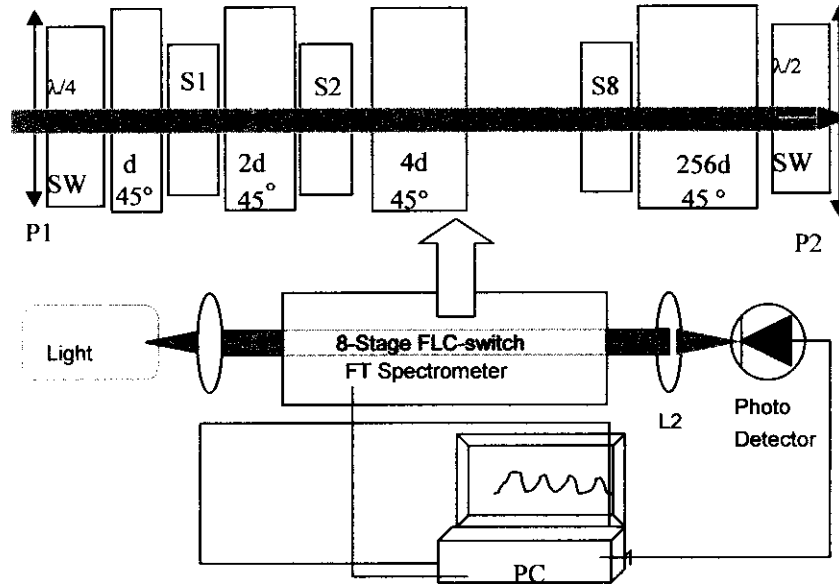


Figure 3. Schematic setup for the 8-stage spectrometer test.

4. BROADBAND EOIFTS DESIGN

The key components determining the bandwidth of the EOIFTS system is the achromatic phase switches. We have developed a new technology to achieve broadband achromatic phase switches. We have modeled the spectral response and optical operation of a 5-plate achromatic half-wave switch working in the near-IR region using proprietary software modeling tools. The schematic of the achromatic half-wave solid-state switch is shown in Figure 4. Four passive Nitto Denko retardation film (NRF) sheets and one FLC switch are used to construct the compound retarder. The retardance for each NRF is a full-wave at 810 nm. The retardance of the FLC switch is a half-wave at 1550nm. An effective achromatic half-wave plate at 45° results from the structure where the orientations of the five waveplates are 7°, 36°, 102°, 36°, and 7°, respectively. The structure where the five orientations are 7°, 36°, 147°, 36°, and 7°, respectively, generates an effective achromatic half-wave plate at 0°.

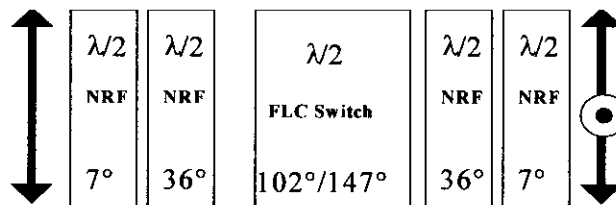


Figure 4. The Schematic of a super-achromatic half-wave switch

A typical simulation result for an effective achromatic half-wave plate at 45° (i.e. with the orientations of the five waveplates 7° , 36° , 102° , 36° and 7° , respectively) is shown in Figure 5. The spectral range with leakage less than 0.5% is from 1161 nm to 2413 nm. This “super-achromatic” design is close to the requirement from 1 to 2.5 μm . By optimizing the angle orientations, the super-band can be further improved (though still short of the perfect requirement from 1 to 2.5 μm). Figure 6 shows a result with the orientations of the five waveplates 7° , 35.8° , 101.5° , 35.8° and 7° , respectively. The spectral range with leakage less than 0.5% is from 1155 nm to 2437 nm.

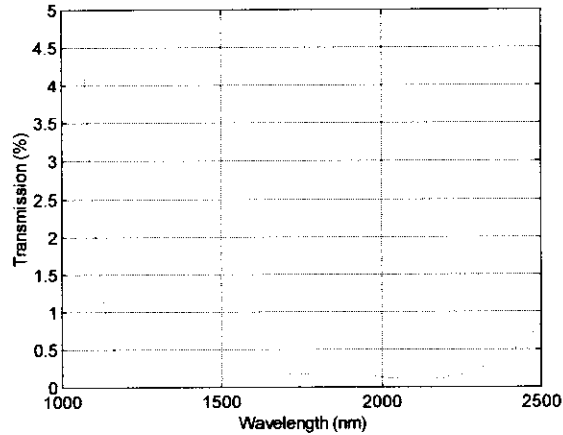


Figure 5. Simulation of the super-achromatic half-wave switch with the orientations of the five waveplates: 7° , 36° , 102° , 36° and 7° .

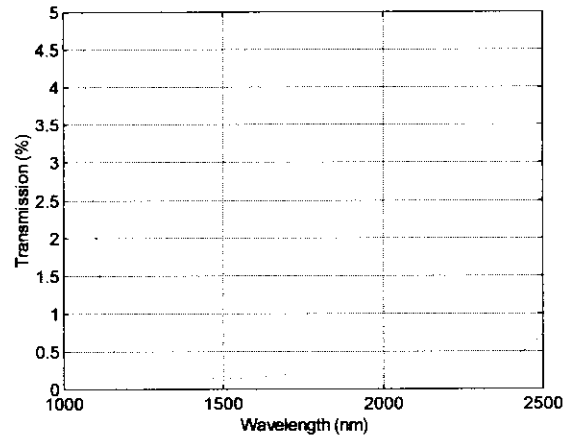


Figure 6. Simulation of the super-achromatic half-wave switch with the orientations of the five waveplates: 7° , 35.8° , 101.5° , 35.8° and 7° .

4.1 FABRICATION OF ACHROMATIC HALF-WAVE SWITCHES

Half-wave FLC cells centered at 1550 nm were fabricated with a pair of CaF₂ ITO-coated substrates, filled with FLC Felix-018. Nylon was used as the alignment material. We paid attention to four factors that affect the FLC alignment: 1) mechanical buffing pressure, 2) filling hole size, 3) heating temperature, and 4) soak time. A moderate pressure is required to buff the nylon. Buffing too hard will deteriorate the surface of nylon coating and too light can not produce enough anchor energy to align the FLC. A tiny fill hole is the choice to make a better FLC cell. The flow speed of FLC across the cell will be slow so that it can minimize the flow alignment that will result in a defect. The heating temperature is kept a few degrees above isotropic state of the Felix FLC. Higher temperature will increase the corrosion of FLC to attack the nylon layer. When FLC was filled in the gap between two windows, the surface tension will pull the substrates together. The windows were deformed and a couple of optical fringes were observed. The cell needed to be soaked at isotropic temperature for a while to relax. If the soak time is too long it will also

create the defect. Less than one-hour soak time is restricted for this FLC material. Defect-free FLC cells were obtained by taking care of the above factors. The product yield was better than 60%.

Figure 7 shows a typical switching result of the achromatic switches we fabricated. During the experimental measurements, the LC switch was toggled at a rate of 0.7 Hz. The switch speed of the modulator can be fast, on the order of sub-ms, with low operating voltages (<5V). It can be seen that the leakage is very low for the spectral range from 1.1 μm to 2.5 μm .

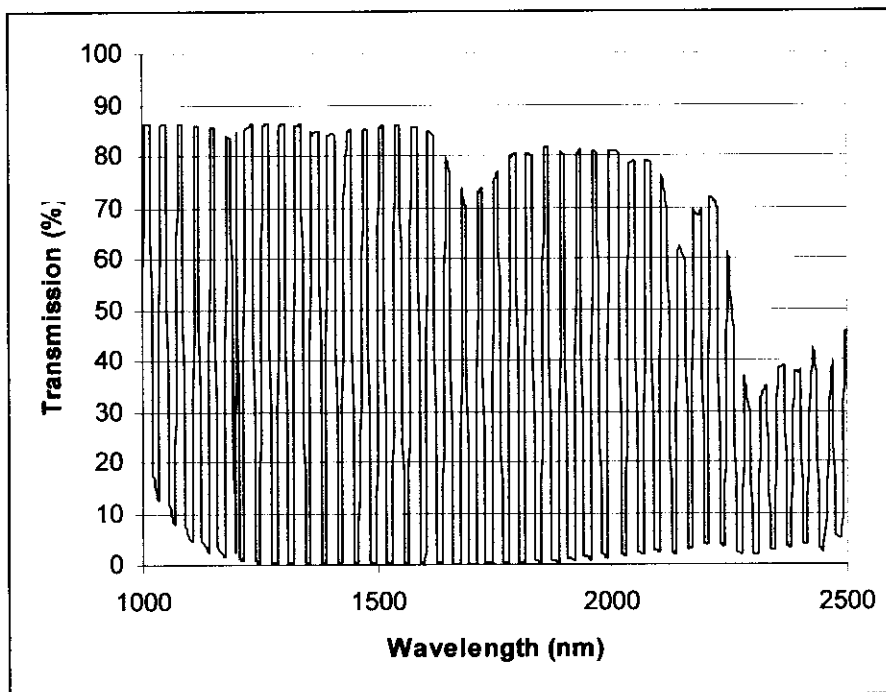


Fig. 7. Achromatic ON and OFF transmission of the achromatic half-wave switch

We also tested the switch speed of the achromatic FLC half-wave switch. Good switch speed (sub-ms) was achieved as typically shown in Figure 7. The rise and fall switching speed are 449 μs and 354 μs , respectively. The extinction ratio was measured to be 600:1.

4.2 FABRICATION OF YVO4 PASSIVE RETARDERS

YVO₄ crystals with a high-birefringence ($\Delta n=0.204$ @1550nm) and broad IR transmission band (0.40-5.0 μm) have been chosen as the multiple-wave passive retarders. The high-birefringence would greatly reduce its thickness for a desired time delay in the near IR range. For an 8-stage Fourier Transform Spectrometer setup, nine passive multi-wave retarders are required. We ordered from United Crystals Inc. ten YVO₄ retarders with retardation of 1λ , 2λ , 4λ , 8λ , 16λ , 32λ , 64λ , 128λ , 256λ , and 512λ at central wavelength of 1550 nm. Accurate single-plate retarders at 64λ , 128λ , 256λ , and 516λ were fabricated. Lower-order YVO₄ wave retarders less than 64 waves (1, 2, 4, 8, 16, 32 waves) are too thin and fragile to be fabricated in a single piece.

5. INTEGRATION OF THE FOURIER TRANSFORM SPECTROMETER

The 8-stage setup is shown in Figure 3. Multiple optical delays are generated via 8 achromatic half-wave FLC switches (S1, S2, S3... and S8) put among nine YVO₄ passive wave retarders of various delays. The ninth

achromatic half-wave switch ($\lambda/2$ SW) was used to generate a 0 or π phase retardation. An achromatic $\lambda/4$ switch ($\lambda/4$ SW) was used to shift the system to additional $\pm\pi/2$ phase. An interface control program was written to apply voltages (± 5 V) on the FLC switches, and to acquire signals. Either a diode laser at 1550 nm wavelength or a broadband Amplified Spontaneous Emission (ASE) source at 1550 nm was used as light source and a single photodiode working in the range from 0.9 to 2.6 μm as the light detector. The signal from the detector was acquired by an A/D board in a computer.

A UEIDAQ PD2-AO-10/16 PCI analog output board is chosen for analog signals to drive the FLC switches. This multi-channel electronics driver can provide 10 analog output channels for driving 9 FLC switches (S1, S2, S3... S7, S8 and $\lambda/2$ -SW). A model LJUI2 USB analog input board from LabJack was purchased to act as the A/D interface for reading spectrum signal from the photo diode. A PC can interface the driver and generate any code to the driving scheme. Control software was developed using Labwindow /CVI tool. The software has the ability to control DIO and 16 bit A/D cards. It can send voltage signal to the electronics driver and read spectrum signal from photo diode.

The LC devices are switched in a “complementary sequence,” so that no LC devices are biased in one polarity for longer than two states of the order switch (1 and 0 stand for +5V and -5V driving voltages, respectively). For an illustration, the four-stage (five half-wave switches including the $\lambda/2$ -SW) system is given by thirty two states:

Sample	Voltage	Sample	Voltage
1	00000	17	01010
2	11111	18	10101
3	00001	19	01011
4	11110	20	10100
5	00010	21	01110
6	11101	22	10001
7	00011	23	01111
8	11100	24	10000
9	01100	25	01010
10	10011	26	10101
11	01101	27	01011
12	10010	28	10100
13	01110	29	01000
14	10001	30	10111
15	01111	31	01001
16	10000	32	10110

The cosine and sine components of the Fourier transform spectrum are obtained when the quarter wave retarder ($\lambda/4$ SW) is aligned to 0°, or 45°, respectively. In each case, 32 output data are collected. A total of 64 outputs are expected for one FTS run.

The software programmed with Mathcad contains the algorithm for spectrum recovery for the data obtained in the experiments. The algorithm has the operation for Fourier transformation, incorporated the dispersion effect of either the quartz or YVO4 crystals.

6. EXPERIMENTAL TESTING RESULTS

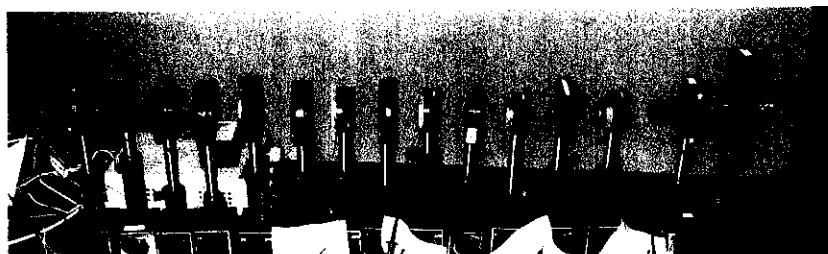


Figure 8. Photo of Lab setup for the 3-stage spectrometer.

We have built and test EOIFTS system in lab. A photo of a 3-stage EOIFTS system setup is shown in Figure 8. During the experimental investigation, we have initially fabricated 7 accurate YVO₄ wave retarders at 8-wave, 16-wave, 32-wave, 64-wave, 128-wave, 256-wave and 516-wave fabricated, we first had a 6-stage FTS setup. An ASE source at 1550 nm was tested. A typical measured spectrum is shown in Figure 9. The ASE lineshape at 1550 nm is clearly identified. We then had a preliminary testing for the 7-stage and 8-stage setup by adding in the 2-wave, and 4-wave retarders. The results are not so consistent possibly due to the inaccuracies of the lowest-wave compounds at 2-wave, and 4-wave. More through experiments are on-going .

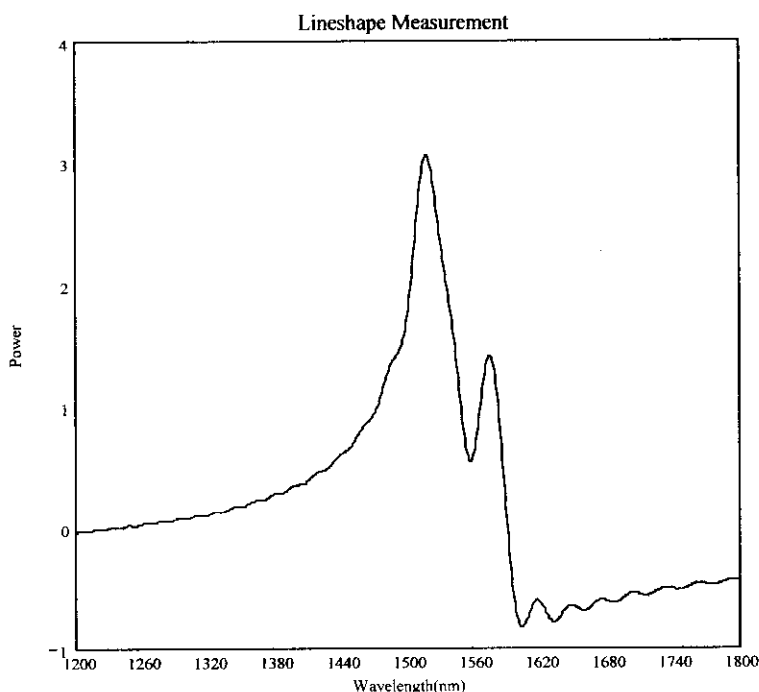


Figure 9. The measured spectrum of a 1550-nm ASE broadband source using the 6-stage FTS with YVO₄ retarders.

6. SUMMARY

We have developed an innovative electro-optic Fourier transform spectrometer. Following the initial, proof-of-principle demonstration of a 3-stage IR FTS breadboard in 2004, we have further developed an 8-stage engineering breadboard. We have selected YVO₄ as the phase retarders due to its high-birefringence and flat spectral response.

The thickness YVO_4 is 20 times less than that of quartz (used in previous system). The major components (achromatic half-wave switches and YVO_4 retarders) design, fabrication and test results have been reported. The experimental result of spectral data capture of that of a test diode laser source and the follow-on recovery through an inverse Fourier transform have also been accomplished. We will continue to integrate a multiple stage system with ultrahigh resolution. Imaging optics will also be included into the system to enable hyperspectral imaging applications

5. ACKNOWLEDGMENTS

The research described in this paper was carried out by the Jet Propulsion Laboratory, California Institute of Technology, under a contract with the National Aeronautics and Space Administration. The authors wish to express their sincere thanks to Dr. Geoffrey helpful technical discussions.

6. REFERENCES

- [1] G. D. Sharp *et al.* "Polarization Interferometer Using Multi-order and Zero-order Birefringence Switches", U.S. Patent Application 08/948,860, Claims allowed (10/12/99).
- [2] G. D. Sharp, P. Wang, S. Serati, T. Ewing, "Liquid Crystal Fourier Transform Spectrometer", SPIE AeroSense, (1998).
- [3] P. Fellgett, Cambridge University thesis, 1951.
- [4] G. D. Sharp, K. M. Johnson, "Liquid crystal achromatic compound retarder", U. S. Patent 5,658,490
- [5] Xiaowei Xia, Steve Serati, Teresa Ewing, Ping Wang, "A massively parallel liquid crystal Fourier transform spectrometer", Final report of Air Force Phase-II SBIR project, Dec. 1999.